

# Magnetic Hysteresis and Complex Initial Permeability of Cr<sup>3+</sup> Substituted Mn-Zn Ferrites

F. Alam<sup>1\*</sup>, M. L. Rahman<sup>2</sup>, M. H. R. Khan<sup>3</sup>, A. K. M. Akther Hossain<sup>4</sup>

<sup>1</sup>Department of Physical Sciences, School of Engineering and Computer Science, Independent University, Dhaka, Bangladesh

<sup>2</sup>Department of Mathematics and Natural Sciences, BRAC University, Dhaka, Bangladesh

<sup>3</sup>Department of Arts and Sciences, Ahsanullah University of Science and Technology, Dhaka, Bangladesh

<sup>4</sup>Departments of Physics, Bangladesh University of Engineering and Technology, Dhaka, Bangladesh

Email: \*[farhadiub@gmail.com](mailto:farhadiub@gmail.com)

Received 20 May 2014; revised 18 June 2014; accepted 11 July 2014

Copyright © 2014 by authors and Scientific Research Publishing Inc.

This work is licensed under the Creative Commons Attribution International License (CC BY).

<http://creativecommons.org/licenses/by/4.0/>



Open Access

---

## Abstract

The impact of Cr<sup>3+</sup> ion on the magnetic properties of Mn<sub>0.50</sub>Zn<sub>0.50</sub>Cr<sub>x</sub>Fe<sub>2-x</sub>O<sub>4</sub> (with x = 0.0, 0.1, 0.2, 0.3, 0.4 and 0.5) has been studied. Ferrite samples were synthesized by combustion method and sintered at various temperatures (1250°C, 1300°C and 1350°C). The structural properties were investigated by means of X-ray diffraction patterns and indicated that the samples possess single phase cubic spinel structure. The lattice parameter decreases with the increase in Cr<sup>3+</sup> content, as the ionic radius of Cr<sup>3+</sup> ion is smaller than that of Fe<sup>3+</sup>. The average grain size (D), bulk density ( $\rho_B$ ) and initial permeability ( $\mu'_i$ ) decreases with increase in Cr<sup>3+</sup> content whereas porosity follows its opposite trend. The  $\rho_B$  was found to increase with increase in Cr<sup>3+</sup> content as the sintering temperature ( $T_s$ ) is increased from 1250°C to 1350°C. The  $T_s$  affects the densification, grain growth and  $\mu'_i$  of the samples. The  $\mu'_i$  strongly depends on average grain size, density and intragranular porosity. The B-H loops of the compositions were measured at room temperature. The saturation magnetization ( $M_s$ ), coercivity ( $H_c$ ) and hysteresis losses were studied as a function of Cr<sup>3+</sup> content. The  $M_s$  was found to decrease with the increase of Cr<sup>3+</sup> content, which is attributed to the dilution of A-B interaction.

## Keywords

Mn-Zn Ferrites, Initial Permeability, Saturation Magnetization, Hysteresis Loss

---

\*Corresponding author.

## 1. Introduction

Polycrystalline mixed spinel ferrites are very attractive for their various potential applications. Manganese zinc and substituted manganese zinc ferrites are technologically important materials due to their high magnetic permeability, high saturation magnetization, high resistivity and low power losses. These ferrites have been extensively used in electronic applications such as transformers, choke coils, noise filters, recording heads, multi-layer chip inductor, electromagnetic wave absorbers etc. [1]-[5]. Crystallographically, spinel ferrites have tetrahedral A-site and octahedral B-site in  $AB_2O_4$  crystal structure. It shows various magnetic and electrical properties depending on the type of cations and their distribution between the two interstitial sites. Desired electrical and magnetic properties of soft ferrites can be tailored by controlling the different types and amount of substitutes and by choosing suitable synthesis technique [6]-[9]. A large number of mixed ferrites like Mn-In-Zn [10], Ni-Mn-Zn [11], Mg-Mn-In and Mg-Mn-Cr [12], Ni-Zn-Cr [13], Cd-Mg-Cr [14] have been prepared by various processing techniques and their structural, electrical and magnetic properties have been reported. Properties of ferrites are sensitive to the processing technique which can play a very crucial role in defining the structural and magnetic properties. Many researchers have studied the effect of the substitution of  $Cr^{3+}$  in the spinel structure of ferrites [15]-[17]. However, there are no reports in the literature about  $Cr^{3+}$  substitution for  $Fe^{3+}$  in Mn-Zn ferrites obtained by combustion technique. Compared with the other synthesis methods, the combustion method offers advantages of being fast and simple, short preparation duration and low energy consumption. The present paper therefore reports on a study of  $Cr^{3+}$  substituted Mn-Zn ferrite produced by combustion synthesis, and on its structural and magnetic characterization.

## 2. Experimental

The nominal chemical compositions of  $Mn_{0.50}Zn_{0.50}Cr_xFe_{2-x}O_4$  (with  $x = 0.0, 0.1, 0.2, 0.3, 0.4$  and  $0.5$ ) were synthesized by combustion method. All the raw materials used in this reaction were of analytical grade. The proper amounts of powders of  $Cr(NO_3)_3 \cdot 9H_2O$ ,  $Zn(NO_3)_2 \cdot 6H_2O$ ,  $MnCl_2 \cdot 4H_2O$  and  $Fe(NO_3)_3 \cdot 9H_2O$  were dissolved in ethanol (GR grade). Then the solution were placed at a constant temperature bath ( $\sim 70^\circ C$ ) followed by an ignition and formed a fluffy loose product of the desired composition. The resultant powders were calcined at  $900^\circ C$  for five hours in air. The grounded fine powders were mixed with binder, and then pressed into disk- and toroid-shaped samples. The samples prepared from each composition were sintered at  $1250^\circ C$ ,  $1300^\circ C$  and  $1350^\circ C$  for five hours in air. During sintering, temperature ramps were  $10^\circ C/min$  for heating and  $5^\circ C/min$  for cooling. Surfaces of all sintered samples were polished and thermally etched. The crystalline structure and phase of the compositions were identified using X-ray diffraction (XRD) patterns obtained using  $CuK\alpha$  radiation ( $\lambda = 1.54178\text{\AA}$ ) for  $2\theta$  value. The lattice parameter for each composition was determined using Nelson-Riley function [18]. The  $\rho_B$ , of the samples were determined using the Archimedes principle. The theoretical density ( $\rho_{th}$ ) was calculated using the expression:  $\rho_{th} = (8M/N_A a_0^3)$ , where  $N_A$  is Avogadro's number,  $M$  is the molecular weight of the composition and  $a_0$  is the lattice parameter. The porosity ( $P$ ) was calculated from the relation

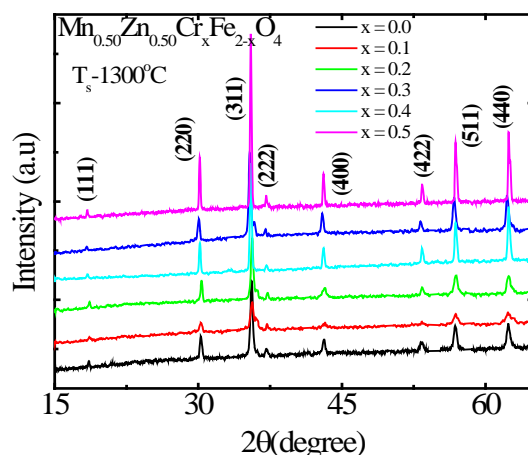
$P(\%) = \{(\rho_{th} - \rho_B)/\rho_{th}\} \times 100$ . The samples were visualized under a high-resolution optical microscope (Olympus DP-70) and then photographed. Average grain sizes of the samples were determined from optical micrographs by linear intercept technique. The frequency dependent initial permeability spectra were determined using Agilent Impedance analyzer (Agilent 4294A) on toroid shaped samples. 4 turns of enameled copper wire were wound on the toroid and the inductance ( $L_s$ ) was measured at room temperature in the frequency range 20 Hz - 120 MHz. The  $\mu'_i$  and the imaginary part ( $\mu''_i$ ) of the complex initial permeability were calculated using the following relations  $\mu'_i = L_s/L_o$ , and  $\mu''_i = \mu'_i \tan \delta$ , where  $L_o = (\mu_o N^2 h/2\pi) \ln(r_o/r_i)$ .  $L_o$  is the inductance of the winding coil without the sample core,  $N$  is the number of turns of the coil,  $h$  is the thickness,  $r_o$  is the outer radius and  $r_i$  is the inner radius of the toroid-shaped sample. The relative quality factor,  $Q$  was calculated from the relation:  $Q = \mu'_i/\tan \delta$ , where  $\tan \delta$  is the loss factor. The DC magnetization measurements were made using the SQUID magnetometer (MPMS-5S; Quantum design Co. Ltd.). B-H loops measurements were performed at room temperature ( $20^\circ C$ ) using an Automatic Magnetic Hysteresis Graph Tracer (Model no. AMH-300, Laboratorio Elettrofisico, Italy). The B-H loops were traced from the toroid shaped specimens with primary and secondary windings of 40:10 ratio of enamelled copper wire using a computer assisted hysteresis loop tracer at a constant frequency 1 kHz and sufficient high applied field to get magnetic saturation.

### 3. Results and Discussion

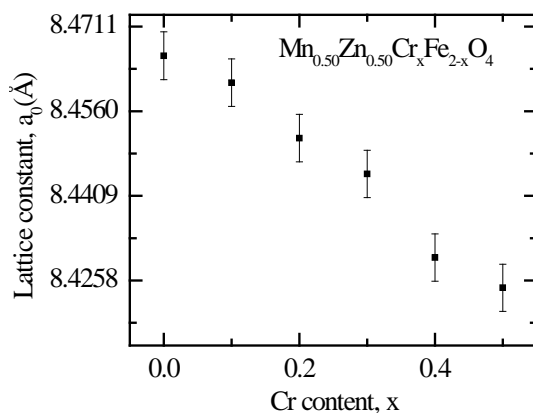
#### 3.1. Lattice Parameter, Density and Porosity

**Figure 1** depicts the X-ray diffraction patterns of various chromium-substituted Mn-Zn ferrites. The patterns exhibit typical reflection of (111), (220), (311), (222), (400), (422), (511) and (440) planes indicating the formation of cubic spinel structure of manganese ferrite. All the diffraction peaks comply with the standard peaks of cubic spinel ferrites. No secondary peaks were detected in XRD patterns of above mentioned samples which ensured the phase purity of each composition. The lattice parameter was determined by using the Nelson-Riley function, which can be expressed as  $F(\theta) = 1/2 [\cos^2 \theta / \sin \theta + \cos^2 \theta / \theta]$ , where  $\theta$  is the Bragg's angle. The exact values of lattice parameter of each sample was estimated from the extrapolation of all peaks to  $F(\theta) = 0$  or  $\theta = 90^\circ$ . As the  $\text{Cr}^{3+}$  substitution increases, the lattice parameter decreases as shown in **Figure 2**. It is due to the fact that the ionic radius of substituting  $\text{Cr}^{3+}$  ( $0.62\text{\AA}$ ) is less than that of  $\text{Fe}^{3+}$  ( $0.64\text{\AA}$ ) [19] [20]. Taking into consideration the preference of  $\text{Cr}^{3+}$  to the octahedral site, the partial replacement of  $\text{Fe}^{3+}$  by  $\text{Cr}^{3+}$  causes a slight effect on the unit cell dimensions [21]. Similar result has been reported in  $\text{Cr}^{3+}$  doped Ni-Zn ferrite prepared by combustion synthesis [13]. The lattice parameter, estimated from XRD patterns is tabulated in **Table 1** along with density, porosity, average grain size and relaxation frequency for various compositions.

**Figure 3** shows the effects of  $\text{Cr}^{3+}$  substitutions on bulk density and porosity in  $\text{Mn}_{0.50}\text{Zn}_{0.50}\text{Cr}_x\text{Fe}_{2-x}\text{O}_4$  ferrites. The  $\rho_B$  decreases with increase in  $\text{Cr}^{3+}$  content, while porosity increases for  $\text{Cr}^{3+}$  substitutions. The decrease in  $\rho_B$  can be attributed to the difference in atomic weight and density of the ferrite components. The atomic weight and density of  $\text{Cr}^{3+}$  ( $51.996$  amu and  $7.19$  g/cm<sup>3</sup>) is less than that of  $\text{Fe}^{3+}$  ( $55.85$  amu and  $7.87$  g/cm<sup>3</sup>) [22]. The



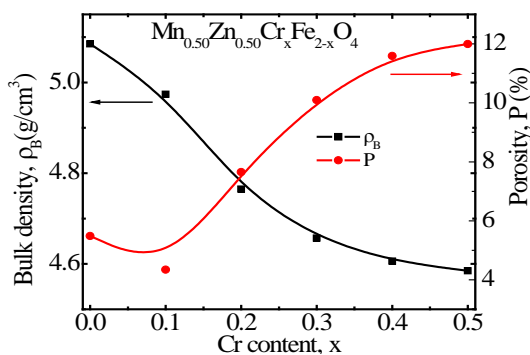
**Figure 1.** The XRD patterns for  $\text{Mn}_{0.50}\text{Zn}_{0.50}\text{Cr}_x\text{Fe}_{2-x}\text{O}_4$  with  $x = 0.0, 0.1, 0.2, 0.3, 0.4$  and  $0.5$ .



**Figure 2.** The variation of lattice parameter with  $\text{Cr}^{3+}$  content ( $x$ ) for various  $\text{Mn}_{0.50}\text{Zn}_{0.50}\text{Cr}_x\text{Fe}_{2-x}\text{O}_4$  samples.

**Table 1.** The lattice parameter, density, porosity, average grain size, real part of initial permeability, coercive field, and room temperature saturation magnetization of various  $\text{Mn}_{0.50}\text{Zn}_{0.50}\text{Cr}_x\text{Fe}_{2-x}\text{O}_4$  sintered at various temperatures in air for 5 h.

$x$	$T_s$ (°C)	$a_0$ (Å)	$\rho_{th}$ (g/cm <sup>3</sup> )	$\rho_B$ (g/cm <sup>3</sup> )	$P$ (%)	$\langle D \rangle$ (μm)	$\mu'_i$ at (1 MHz)	$H_c$ (A/m)	$M_s$ at 1 T (emu/g)
	1250			4.652	13.5				
0.0	1300	8.4659	5.38	5.085	5.48	5.7	299	33	54.7
	1350			5.199	3.36				
	1250			4.536	12.7				
0.1	1300	8.4611	5.20	4.974	4.3	4.6	281	34	51.1
	1350			5.026	3.34				
	1250			4.519	12.4				
0.2	1300	8.4512	5.16	4.765	7.6	4.4	219	39	45.7
	1350			4.969	3.7				
	1250			4.371	15.6				
0.3	1300	8.4448	5.18	4.657	10	3.9	191	40	43.5
	1350			4.93	4.8				
	1250			4.296	17.5				
0.4	1300	8.4299	5.21	4.606	12	3.4	181	42	32.5
	1350			4.835	7.18				
	1250			4.235	18.7				
0.5	1300	8.4245	5.21	4.585	12	3.2	82	63.6	27
	1350			4.776	8.33				

**Figure 3.** The variation of bulk density and porosity as a function of  $\text{Cr}^{3+}$  content ( $x$ ) for various  $\text{Mn}_{0.50}\text{Zn}_{0.50}\text{Cr}_x\text{Fe}_{2-x}\text{O}_4$  sintered at 1300°C.

increase in porosity with the addition of  $\text{Cr}^{3+}$  content may be due to the creation of more cation vacancies with the reduction of oxygen vacancies [23]. It is found that the bulk densities are smaller in magnitude than corresponding theoretical densities. This may be due to the presence of pores in the samples [24].

**Figure 4** shows the variation of  $\rho_B$  and  $P$  for  $\text{Mn}_{0.50}\text{Zn}_{0.50}\text{Cr}_{0.20}\text{Fe}_{1.8}\text{O}_4$  sintered at various sintering temperatures. It is noticed that the  $\rho_B$  of  $\text{Mn}_{0.50}\text{Zn}_{0.50}\text{Cr}_x\text{Fe}_{2-x}\text{O}_4$  ( $x = 0.20$ ) increases with increase in sintering temperature. On the other hand, porosity has the opposite trend. It is also noticed that the  $\rho_B$  for all other compositions increases with increase in sintering temperature, while the porosity of these compositions exhibit opposite behavior which has been tabulated in the **Table 1**. The increases in density with sintering temperature are expected.

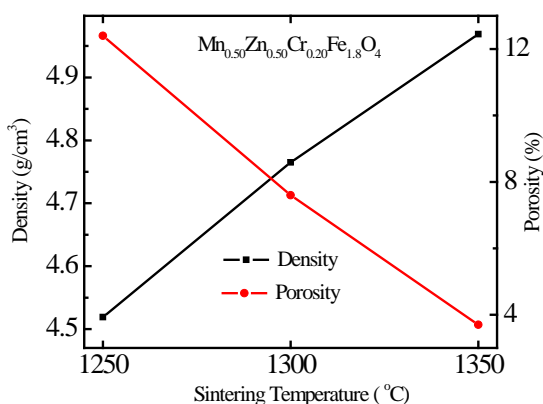


**Figure 4.** The variation of bulk density and porosity with sintering temperature for  $\text{Mn}_{0.50}\text{Zn}_{0.50}\text{Cr}_{0.20}\text{Fe}_{1.8}\text{O}_4$ .

This is because during the sintering process, the thermal energy generates a force that drives the grain boundaries to grow over pores, thereby decreasing the pore volume and densifying the material.

### 3.2. Microstructure of $\text{Mn}_{0.50}\text{Zn}_{0.50}\text{Cr}_x\text{Fe}_{2-x}\text{O}_4$

Magnetic properties of ferrites are dependent on their microstructures. Grain size is more important parameter affecting the magnetic properties of ferrites. Grain growth is closely related to the grain boundary mobility. During grain growth there is a competition between the driving force for grain boundary movement and the retarding force exerted by the pores [25]. When the driving force of the grain boundary in each grain is homogeneous, the sintered body attains a uniform grain size distribution. Discontinuous grain growth occurs if this driving force is inhomogeneous. The optical micrographs of  $\text{Mn}_{0.50}\text{Zn}_{0.50}\text{Cr}_x\text{Fe}_{2-x}\text{O}_4$  ferrites are shown in **Figure 5**. Average grain sizes of the samples determined by the linear intercept technique are presented in **Table 1**. The average grain sizes of the samples vary from 5.7  $\mu\text{m}$  to 3.2  $\mu\text{m}$ . The grain size decreases with increasing  $\text{Cr}^{3+}$  substitution. This may be due to the fact that the melting point of Cr (1914°C) is greater than that of iron (1538°C). With the substitution of chromium, the appearance of smaller grains has been observed and when the substitution level is higher the population of smaller grains is dominating over the larger grains. The size of the bigger as well as smaller grains is decreased when the  $\text{Cr}^{3+}$  concentration is higher. From the microstructures, it is also observed that the porosity is increased when the  $\text{Cr}^{3+}$  content is increased [26].

### 3.3. Magnetic Properties of $\text{Mn}_{0.50}\text{Zn}_{0.50}\text{Cr}_x\text{Fe}_{2-x}\text{O}_4$

#### 3.3.1. Frequency Dependence of Complex Permeability

The complex initial permeability spectra for all  $\text{Mn}_{0.50}\text{Zn}_{0.50}\text{Cr}_x\text{Fe}_{2-x}\text{O}_4$  ferrite compositions sintered at various sintering temperatures as a function of frequency are shown in **Figure 6**. The  $\mu'_i$  decrease with increase in  $\text{Cr}^{3+}$  substitution in  $\text{Mn}_{0.50}\text{Zn}_{0.50}\text{Cr}_x\text{Fe}_{2-x}\text{O}_4$  ferrites. Similar trend is followed in  $\text{Cr}^{3+}$  substituted Li-Sb ferrites [26].

The  $\mu'_i$  remains steady up to a certain frequency, known as relaxation frequency ( $f_r$ ). It is also noticed that there is a decrease in  $\mu'_i$  and increase in  $\mu''_i$  above the  $f_r$ . The  $\mu'_i$  of the samples decrease but the  $f_r$  shifted to higher values as result of  $\text{Cr}^{3+}$  substitutions at higher sintering temperature. The  $\mu'_i$  of a ferromagnetic material depends on many factors like reversible displacement of domain walls, bulging of domain walls as well as microstructural parameters like average grain size, intragranular porosity, etc. [27]. Perduijin and Peloschek [28] and Roess *et al.* [29] found a linear relation between the  $\mu'_i$  and grain size in Mn-Zn ferrites. The  $\mu'_i$  being sensitive to many parameters, it is still difficult to draw a specific conclusion for variation of  $\mu'_i$  with concentration. However  $\mu'_i$  is found to decrease with decreasing of grain size. The  $\mu'_i$  of ferrite follows  $\mu'_i \propto (M_s^2 D / \sqrt{K_1})$ , where  $M_s$  is the saturation magnetization is,  $K_1$  is the magnetocrystalline anisotropy constant and  $D$  is the average grain diameter. The decrease in  $\mu'_i$  with increase in  $\text{Cr}^{3+}$  substitution can be attributed to the decrease in grain size and  $M_s$  which has been discussed in DC magnetization section. Decrease in grain size also results in a decrease in the number of domain walls in each grain. The onset of relaxation frequency (due to domain wall oscillations) is drifting towards the higher side with the increase in  $\text{Cr}^{3+}$  concentration

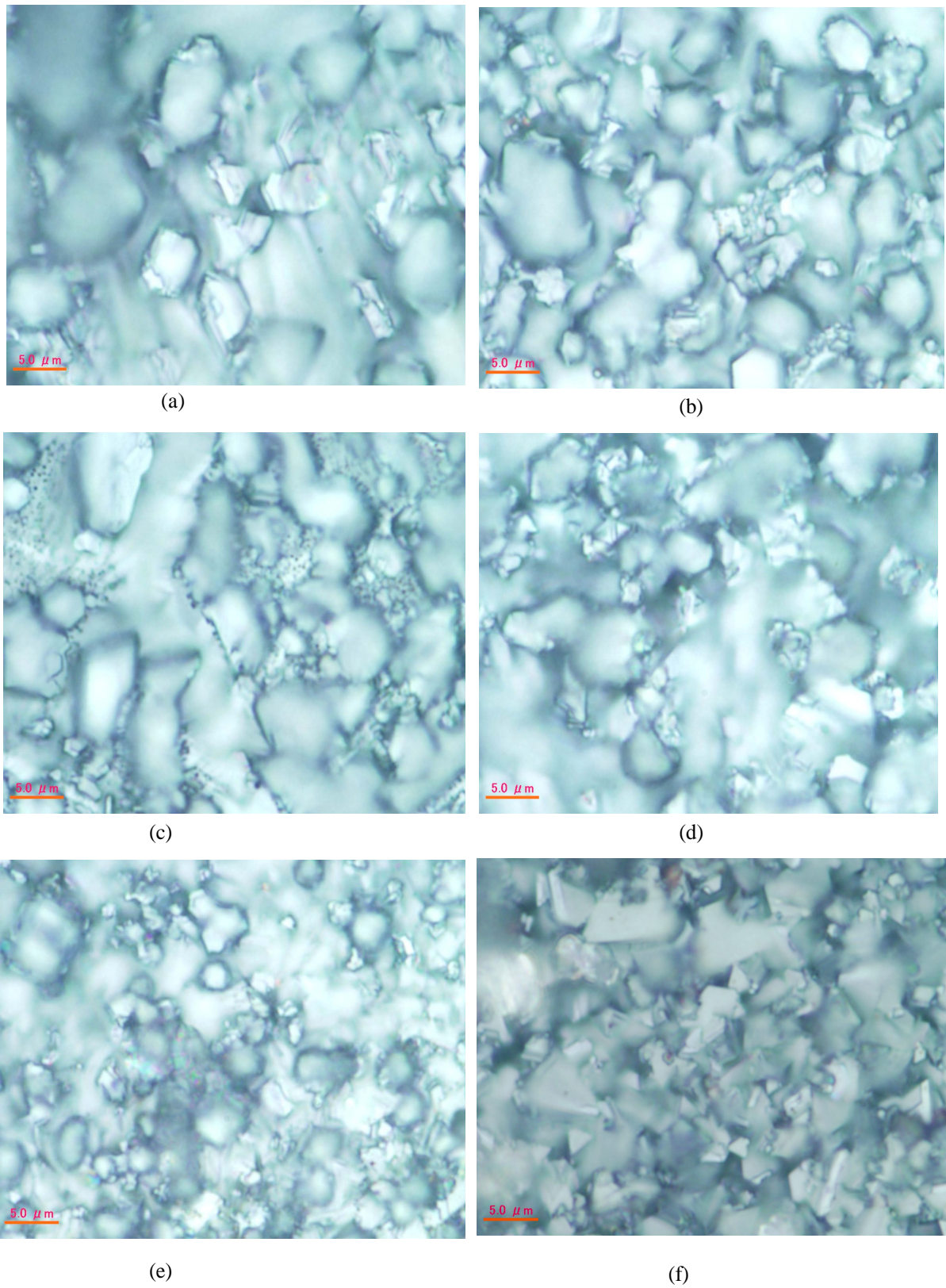


**Figure 5.** The optical micrographs of  $\text{Mn}_{0.50}\text{Zn}_{0.50}\text{Cr}_x\text{Fe}_{2-x}\text{O}_4$  ferrites: (a)  $x = 0.0$ ; (b)  $x = 0.1$ ; (c)  $x = 0.2$ ; (d)  $x = 0.3$ ; (e)  $x = 0.4$  and (f)  $x = 0.5$  sintered at  $1250^\circ\text{C}$ .

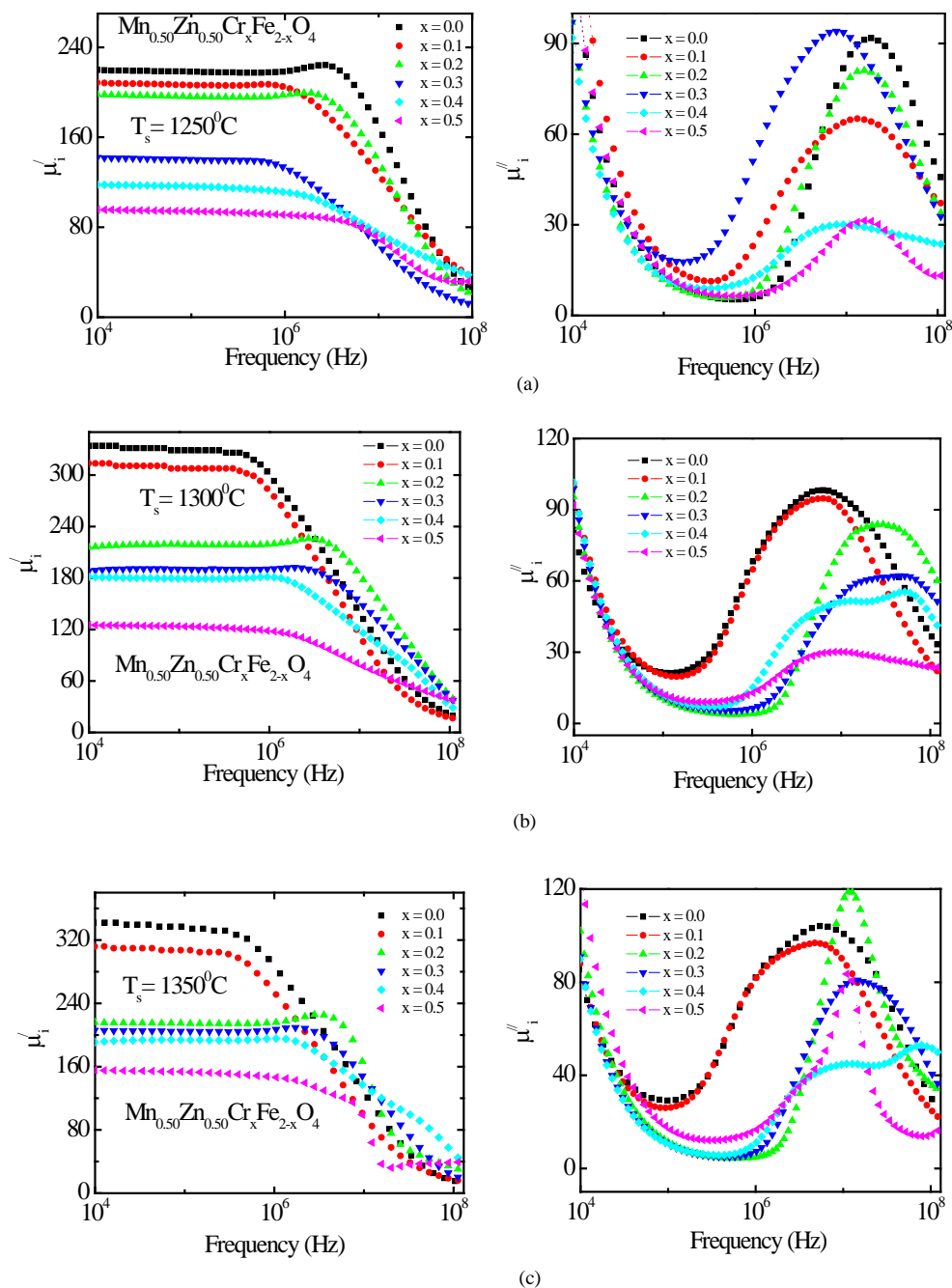


**Figure 6.** The variation of  $\mu'_i$  and  $\mu''_i$  with frequency for  $Mn_{0.50}Zn_{0.50}Cr_xFe_{2-x}O_4$  samples sintered at temperatures (a) 1250 (b) 1300 and (c) 1350°C in air.

or decrease in  $\mu'_i$ . This agrees well with the Globus model [30].

### 3.3.2. Frequency Dependence of Relative Quality Factor

**Figure 7** shows the frequency dependence of relative quality factor (RQF) of the samples sintered at (a) 1300°C and (b) 1350°C. The RQF increases with an increase in frequency, showing a peak and then decreases. The variation of RQF with frequency showed a similar trend for all the samples. It is seen that RQF decreases beyond 0.2 MHz *i.e.* the loss tangent is minimum up to 0.2 MHz and then it rises rapidly. The loss is due to lag of domain wall motion with the applied alternating magnetic field and is attributed to various domain effect, which

include non-uniform and non-repetitive domain wall motion, domain wall bowing, localized variation of flux density, nucleation and annihilation of domain wall [31]. The peak corresponding to maxima in quality factor shifts to higher frequency as Cr<sup>3+</sup> content increases up to x = 0.20, after that it decreases. RQF has the maximum value for Mn<sub>0.50</sub>Zn<sub>0.50</sub>Cr<sub>0.20</sub>Fe<sub>1.8</sub>O<sub>4</sub> sintered at 1300°C.

### 3.3.3. DC Magnetization

The magnetization (*M*) as a function of applied magnetic field (*H*) for various Mn<sub>0.50</sub>Zn<sub>0.50</sub>Cr<sub>x</sub>Fe<sub>2-x</sub>O<sub>4</sub> (with x = 0.0, 0.1, 0.2, 0.3, 0.4 and 0.5) measured at room temperature (300 K) are shown in Figure 8. The magnetization of all samples increases linearly with increasing the applied magnetic field up to 0.1 T. Beyond this applied field magnetization increases slowly and then saturation occurs. The saturation magnetization, *M<sub>s</sub>*, for all sample are determined by the extrapolation of magnetization curve to  $\mu_0 H = 0$ .

L. Néel [32] considered three kinds of exchange interactions between unpaired electrons of two ions lying: (i) both ions at A sites (AA interaction), (ii) both ions at B sites (BB interaction), and (iii) one at a site and the other at B site (AB interaction). AB interaction strongly predominates over AA and BB interactions. The AB interaction aligns all the magnetic spins at A site in one direction and those at B site in opposite direction. The net magnetic moment of the lattice is therefore the difference between the magnetic moments of B and A sublattices, i.e.,  $M = M_B - M_A$ . The saturation magnetization is observed to decrease with increasing paramagnetic Cr<sup>3+</sup> content throughout the concentration range studied. It is well known that Cr<sup>3+</sup> ions preferably occupy B sites [33]. As the number of Fe<sup>3+</sup> ions at B sites continuously decreases, the magnetization of B sub lattice decreases which results into the observed decrease in saturation magnetization. A similar decrease was reported in Mn-Zn-Cr [34] and Mg-Mn-Cr ferrites [35].

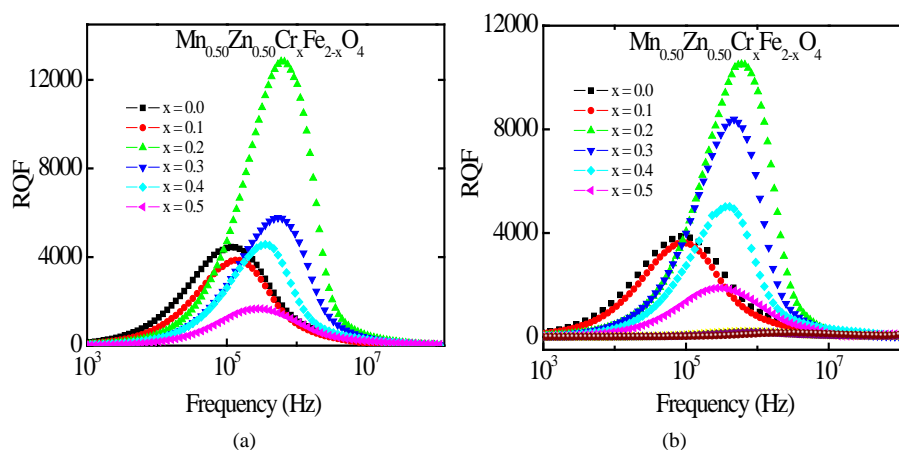


Figure 7. The variation of Relative Quality Factor (RQF) with frequency for Mn<sub>0.50</sub>Zn<sub>0.50</sub>Cr<sub>x</sub>Fe<sub>2-x</sub>O<sub>4</sub> samples sintered at (a) 1300 and (b) 1350°C.

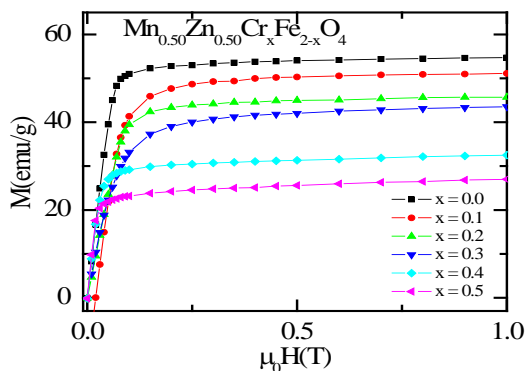
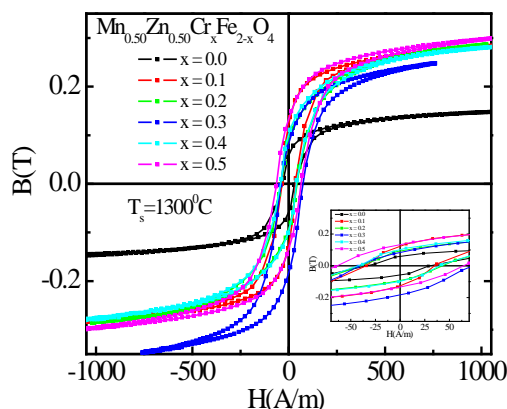
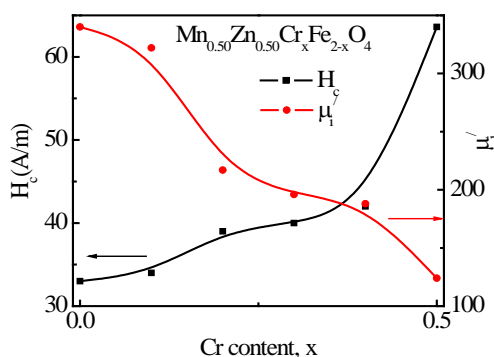


Figure 8. The magnetization (*M*) versus the applied magnetic field (*H*) curves for Mn<sub>0.50</sub>Zn<sub>0.50</sub>Cr<sub>x</sub>Fe<sub>2-x</sub>O<sub>4</sub> at room temperature.



**Figure 9.** B-H loops of polycrystalline  $\text{Mn}_{0.50}\text{Zn}_{0.50}\text{Cr}_x\text{Fe}_{2-x}\text{O}_4$  ferrites at room temperature. The inset B-H loops at low field.



**Figure 10.** The variation of  $H_c$  and  $\mu'_i$  for various  $\text{Mn}_{0.50}\text{Zn}_{0.50}\text{Cr}_x\text{Fe}_{2-x}\text{O}_4$  for various  $\text{Cr}^{3+}$  content.

The hysteresis loops of the Mn-Zn-Cr ferrite were recorded by a computer interfaced hysteresis loop tracer at room temperature at constant frequency  $f = 1$  kHz. **Figure 9** shows the B-H loops of the samples of the composition  $\text{Mn}_{0.50}\text{Zn}_{0.50}\text{Cr}_x\text{Fe}_{2-x}\text{O}_4$  sintered at  $1300^\circ\text{C}$ . The inclusion of  $\text{Cr}^{3+}$  enhances the hysteresis loop, which in turn increased coercive field ( $H_c$ ), favoring its application in high frequency transformer. The addition of  $\text{Cr}^{3+}$  reduced the  $M_s$  as expected as it reduces the density of magnetic ions at B site.  $H_c$  increases due to the increase of magnetocrystalline anisotropy [36]. It is well known that the shape and size of a B-H loop depends not only on the chemical composition but also on several microstructural properties like grain size, porosity and nature of the pores [37].  $H_c$  is inversely proportional to initial permeability  $\mu'_i$  of the ferrite system as shown in **Figure 10**. Our present observations of compositional variation of  $H_c$  with  $\mu'_i$  agree with the reported value [38] [39].

#### 4. Conclusion

Substitution of  $\text{Cr}^{3+}$  in Mn-Zn ferrite results in slight shrinkage of the unit cell.  $D$ ,  $\rho_B$ ,  $\mu'_i$ , as well as  $M_s$  decrease with  $\text{Cr}^{3+}$  content. As  $\mu'_i$  decreases the  $f_r$  of the samples shifts towards the higher frequency up to a particular  $\text{Cr}^{3+}$  content. The  $f_r$  indicates the operational frequency limit of the ferrites in applications, so it is preferable to push this frequency to the higher frequency region. In our present investigation operational frequency range is increased with a particular  $\text{Cr}^{3+}$  substitution. Saturation magnetization decreased with  $\text{Cr}^{3+}$  content whereas  $H_c$  was found to increase at the  $\text{Cr}^{3+}$  rich Mn-Zn ferrites.

#### Acknowledgements

F. Alam would like to acknowledge CASR of Bangladesh University of Engineering and Technology for financing

and Bangladesh Atomic Energy Center, Dhaka for providing B-H loop data. Thanks are also due to M. A. Rahman for valuable discussions for preparation of the manuscript.

## References

- [1] Syue, M.-R., Wei, F.-J., Chou, C.-S. and Fu, C.-M. (2011) *Journal of Applied Physics*, **109**, Article ID: 07A324. <http://dx.doi.org/10.1063/1.3560880>
- [2] Praveena, K., Sadhana, K., Bharadwaj, S. and Murthy, S.R. (2010) *Materials Research Innovations*, **14**, 56-61. <http://dx.doi.org/10.1179/143307510X12599329343727>
- [3] Praveena, K., Sadhana, K., Bharadwaj, S. and Murthy, S.R. (2009) *Journal of Magnetism and Magnetic Materials*, **321**, 2433-2437. <http://dx.doi.org/10.1016/j.jmmm.2009.02.138>
- [4] Subramani, A.K., Kondo, K., Tada, M., Abe, M., Yoshimura, M. and Matsushita, N. (2009) *Journal of Magnetism and Magnetic Materials*, **321**, 3979-3983. <http://dx.doi.org/10.1016/j.jmmm.2009.07.036>
- [5] Latorre-Esteves, M., Cortes, A., Torres-Lugo, M. and Rinaldi, C. (2009) *Journal of Magnetism and Magnetic Materials*, **321**, 3061-3066. <http://dx.doi.org/10.1016/j.jmmm.2009.05.023>
- [6] Albuquerque, A.S., Ardison, J.D., Macedo, W.A.A. and Alves, M.C.M. (2000) *Journal of Applied Physics*, **87**, 4352-4357. <http://dx.doi.org/10.1063/1.373077>
- [7] Selvan, R.K., Augustin, C.O., Berchmans, L.J. and Saraswathi, R. (2003) *Materials Research Bulletin*, **38**, 41-54. [http://dx.doi.org/10.1016/S0025-5408\(02\)01004-8](http://dx.doi.org/10.1016/S0025-5408(02)01004-8)
- [8] Li, F., Liu, J.J., Evans, D.G. and Duan, X. (2004) *Chemistry of Materials*, **16**, 1597-1602. <http://dx.doi.org/10.1021/cm035248c>
- [9] Liu, J.H., Wang, L. and Li, F.S. (2005) *Journal of Materials Science*, **40**, 2573-2575. <http://dx.doi.org/10.1007/s10853-005-2077-6>
- [10] Mathur, P., Thakur, A. and Singh, M. (2008) *Journal of Physics and Chemistry of Solids*, **69**, 187-192. <http://dx.doi.org/10.1016/j.jpics.2007.08.014>
- [11] Singh, A.K., Singh, A.K., Goel, T.C. and Mendiratta, R.G. (2004) *Journal of Magnetism and Magnetic Materials*, **281**, 276-280. <http://dx.doi.org/10.1016/j.jmmm.2004.04.115>
- [12] Laksman, A., Rao, K.H. and Mendiratta, R.G. (2002) *Journal of Magnetism and Magnetic Materials*, **250**, 92-97. [http://dx.doi.org/10.1016/S0304-8853\(02\)00359-1](http://dx.doi.org/10.1016/S0304-8853(02)00359-1)
- [13] Gama, L., Hernandez, E.P., Cornejo, D.R., Costa, A.A., Rezende, S.M., Kiminami, R.H.G.A. and Costa, A.C.F.M. (2007) *Journal of Magnetism and Magnetic Materials*, **317**, 29-33. <http://dx.doi.org/10.1016/j.jmmm.2007.04.007>
- [14] Masti, S.A., Sharma, A.K., Vasambekar, P.N. and Vainganker, A.S. (2006) *Journal of Magnetism and Magnetic Materials*, **305**, 436-439. <http://dx.doi.org/10.1016/j.jmmm.2006.01.229>
- [15] El-Sayed, A.M. (2003) *Materials Chemistry and Physics*, **82**, 583-587. [http://dx.doi.org/10.1016/S0254-0584\(03\)00319-5](http://dx.doi.org/10.1016/S0254-0584(03)00319-5)
- [16] Sankpal, A.M., Suryavanshi, S.S., Kakatkar, S.V., Tengshe, G.G., Patil, R.S., Chaudhari, N.D. and Sawant, S.R. (1998) *Journal of Magnetism and Magnetic Materials*, **186**, 349-356. [http://dx.doi.org/10.1016/S0304-8853\(97\)01156-6](http://dx.doi.org/10.1016/S0304-8853(97)01156-6)
- [17] Rao, K.H., Gaur, N.K., Aggarwal, K. and Mendiratta, R.G. (1982) *Journal of Applied Physics*, **53**, 1122-1126. <http://dx.doi.org/10.1063/1.330525>
- [18] Nelson, J.B. and Riley, D.P. (1945) *Proceedings of the Physical Society*, London, **57**, 160-177. <http://dx.doi.org/10.1088/0959-5309/57/3/302>
- [19] Shanon, R.D. (1976) *Acta Crystallographica Section A*, **32**, 751-767. <http://dx.doi.org/10.1107/S0567739476001551>
- [20] Chae, K.P., Lee, Y.B., Lee, J.G. and Lee, S.H. (2000) *Journal of Magnetism and Magnetic Materials*, **220**, 59-64. [http://dx.doi.org/10.1016/S0304-8853\(00\)00459-5](http://dx.doi.org/10.1016/S0304-8853(00)00459-5)
- [21] Gabal, M.A. and Al Angari, Y.M. (2006) *Journal of Magnetism and Magnetic Materials*, **322**, 3159-3165. <http://dx.doi.org/10.1016/j.jmmm.2010.05.054>
- [22] Kittel, C. (1976) *Introduction to Solid State Physics*. 5th Edition, John Wiley & Sons, Inc., New York.
- [23] Abbas, T., Islam, M.U. and Ashraf, Ch.M. (1995) *Modern Physics Letters B*, **9**, 1419-1426.
- [24] Barakat, M.M., Hanaish, M.A., Olofa, S.A. and Tawfik, A. (1991) *Journal of Thermal Analysis*, **37**, 241-248. <http://dx.doi.org/10.1007/BF02055926>
- [25] Bellad, S.S., Watawe, S.C. and Chougule, B.K. (1999) *Journal of Magnetism and Magnetic Materials*, **195**, 57-64. [http://dx.doi.org/10.1016/S0304-8853\(98\)01073-7](http://dx.doi.org/10.1016/S0304-8853(98)01073-7)

- [26] Laishram, R. and Prakash, C. (2006) *Journal of Magnetism and Magnetic Materials*, **305**, 35-39.  
<http://dx.doi.org/10.1016/j.jmmm.2005.11.037>
- [27] Smit, J. and Wijn, H.P.J. (1959) Ferrites. Philips Technical Library, Eindhoven, 150.
- [28] Perduijn, D.J. and Peloschek, H.P. (1968) *Proceedings of the British Ceramic Society*, **10**, 263.
- [29] Roess, E., Hanke, I. and Moser, E. (1964) *Zeitschrift für Angewandte Physik*, **17**, 504.
- [30] Globus, A., Duplex, P. and Guyot, M. (1971) *IEEE Transactions on Magnetics*, **7**, 617-622.  
<http://dx.doi.org/10.1109/TMAG.1971.1067200>
- [31] Overshott, K.J. (1981) *IEEE Transactions on Magnetics*, **17**, 2698-2700.  
<http://dx.doi.org/10.1109/TMAG.1981.1061648>
- [32] Néel, L. (1948) *Annales de Physique*, **3**, 137-198.
- [33] Rameijin, F.C. (1953) *Philips Research Reports*, **8**, 321.
- [34] Rao, K.H. (1981) Electrical, Magnetic and Mössbauer Studies in Cr, In and Al Doped Zinc-Manganese Ferrites. Ph.D. Thesis, Andhra University, Visakhapatnam.
- [35] Guiland, C. and Creveaux, H. (1950) *Comptes Rendus de l'Académie des Sciences*, **230**, 1256. (France)
- [36] Alone, S.T., Shirsath, S.E., Kadam, R.H. and Jadhav, K.M. (2011) *Journal of Alloys and Compounds*, **509**, 5055-5060.  
<http://dx.doi.org/10.1016/j.jallcom.2011.02.006>
- [37] Singh, A.K., Goel, T.C., Mendiratta, R.G., Thakur, O.P. and Prakash, C. (2002) *Journal of Applied Physics*, **92**, 3872.  
<http://dx.doi.org/10.1063/1.1504493>
- [38] Singh, A.K., Verma, A., Thakur, O.P., Prakash, C., Goel, T.C. and Mendiratta, R.G. (2003) *Materials Letters*, **57**, 1040.
- [39] Liang, T.J., Nien, H.H. and Chen, J.F. (2007) *IEEE Transactions on Magnetics*, **43**, 3816-3827.

Scientific Research Publishing (SCIRP) is one of the largest Open Access journal publishers. It is currently publishing more than 200 open access, online, peer-reviewed journals covering a wide range of academic disciplines. SCIRP serves the worldwide academic communities and contributes to the progress and application of science with its publication.

Other selected journals from SCIRP are listed as below. Submit your manuscript to us via either [submit@scirp.org](mailto:submit@scirp.org) or [Online Submission Portal](#).

